materials

MDPI

Article

Strain Engineered Band Gaps and Electronic Properties in $PbPdO_2$ and $PbPd_{0.75}Co_{0.25}O_2$ Slabs

Yanmin Yang [1,2], Kehua Zhong [1,2], Guigui Xu [3], Jian-Min Zhang [1,2,*] and Zhigao Huang [1,2,*]

1 Fujian Provincial Key Laboratory of Quantum Manipulation and New Energy Materials, College of Physics and Energy, Fujian Normal University, Fuzhou 350117, China; yym@fjnu.edu.cn (Y.Y.); khzhong@fjnu.edu.cn (K.Z.)
2 Fujian Provincial Collaborative Innovation Center for Optoelectronic Semiconductors and Efficient Devices, Xiamen 361005, China
3 Concord University College, Fujian Normal University, Fuzhou 350117, China; xuguigui082@126.com
* Correspondence: jmzhang@fjnu.edu.cn (J.-M.Z.); zghuang@fjnu.edu.cn (Z.H.); Tel./Fax: +86-591-2286-7577 (Z.H.)

Received: 17 August 2018; Accepted: 11 October 2018; Published: 16 October 2018

Abstract: Electronic structure and corresponding electrical properties of $PbPdO_2$ and $PbPd_{0.75}Co_{0.25}O_2$ ultrathin slabs with (002) preferred orientation were systematically investigated using first-principles calculations. The calculated results revealed the strain induced evidently the changes of band structure and carrier concentration in both slabs. It was also found that $PbPdO_2$ and $PbPd_{0.75}Co_{0.25}O_2$ ultrathin slabs exhibited evident differences in the external strain dependence of the band gap and charge carrier concentration, which was strongly dependent on bond angle and bond length induced by in-plane anisotropy strain. Interestingly, the carrier concentration of the $PbPd_{0.75}Co_{0.25}O_2$ slab could increase up to 5–6 orders of magnitude with the help of external strain, which could explain the potential mechanism behind the observed colossal strain-induced electrical behaviors. This work demonstrated that the influence of the doping effect in the case of $PbPdO_2$ could be a potentially fruitful approach for the development of promising piezoresistive materials.

Keywords: $PbPdO_2$; strain; band gap; piezoresistance; anisotropic; first-principles calculations

1. Introduction

In the past decade, spin-gapless semiconductors (SGS) have attracted increasing interest because of their unique physical properties, leading to their potential application in electronic devices, such as field-effect transistors, optoelectronics, electronic sensors, and supercapacitors, amongst others [1–6]. Among them, the $PbPdO_2$-based spin gapless semiconductor is considered as a promising candidate because of its non-toxicity, compatibility to the oxide semiconductor devices, and sensitivity to the doping metal elements, electric field, and operation current. Based on local density approximation calculations, the oxide-based $PbPdO_2$ gapless semiconductor was firstly discovered by Wang [4]. Following this, extensive investigations on the electric and magnetic properties of $PbPdO_2$-based semiconductors were carried out theoretically and experimentally. Wang et al. studied the roles of both electrical current and magnetic field on the resistivity of $PbPd_{0.75}Co_{0.25}O_2$ thin films, and unusual colossal electroresistance and magnetoresistance were observed [5]. Moreover, the distinct different magnetoresistance effects were observed in $PbPd_{0.9}Cu_{0.1}O_2$ and $PbPd_{0.9}Zn_{0.1}O_2$, which would be attributed to local structure deformation due to Pd/O deficiencies [7]. Based on the bound magnetic polaron (BMP) theory, the potential mechanism behind the observed ferromagnetic, paramagnetic, and antiferromagnetic properties coexisting in Co–doped $PbPdO_2$ film were suggested [8]. It was suggested that Pd–O hybridization in Co–doped $PbPdO_2$ thin films were responsible for the transition

from weak localization and weak anti-localization [9]. Simultaneously, many studies on valence states and band structures have been carried out to understand the mechanism on the observed physical behaviors. For example, Chen et al. revealed that a small band gap of $PbPdO_2$ would be induced by Pd deficiency in composites, resulting in increased hybridization of O(2p)–Pb(6p) and decreased O(2p)–Pd(4d) hybridizations [10]. It was found that Pd–O hybridization would efficiently mediate the magnetic coupling among Co atoms [11]. The ferromagnetism and paramagnetism were found to coexist in the Fe–doped $PbPdO_2$, and the bound magnetic polaron model was used to account for the ferromagnetism origin [12]. Based on the measured electronic structures, $Pb(Pd_{0.9}T_{0.1})O_2$ (T = Mn, Co) oxides were found to be the small-gap semiconductors [13]. In our previous study, it was observed that the external electric field in $PbPdO_2$ slab with (002)-preferred orientation influences sensitively the band gap and carrier concentration, which explains the extraordinary electrical behaviors [14].

Recently, the strain effects on the physical properties of two-dimensional materials were investigated [15–18]. The direct-indirect band gap transition induced by strain was also found in two-dimensional phosphorene, which is explained by the near-band-edge electronic orbital theory [15]. It has been established that the strain induces modulation of the band gap resulting in a piezoresistive effect in silicon [16]. Recently, the piezoresistive effect was also found in single-atomic-layer and atomically thin MoS_2 films [17,18]. Strain dependent carrier concentration is generally characterized with piezoresistive gauge factor. The gauge factor (GF) of piezoresistance can be calculated as follows [18],

$$\mathrm{GF} = \frac{\Delta\rho}{\rho}/\varepsilon \tag{1}$$

where ρ_0 is the resistance without strain and $\Delta\rho$ is change of resistance with strain ε. The resistivity (ρ) is in inverse proportion to carrier concentration (n). As $\varepsilon = 0$, let $n = n_0$; $\varepsilon \neq 0$, let $n = n_\varepsilon$. The gauge factor can be re-expressed as follows,

$$\mathrm{GF} = \frac{\Delta\rho}{\rho}/\varepsilon \propto \left(\frac{n_0}{n_\varepsilon} - 1\right)/\varepsilon \tag{2}$$

In $PbPdO_2$-based composites, different preparation and processing methods result unavoidably in different microstructure and strain states, which consequently influences the band gap, carrier concentration, and corresponding electrical properties. Specifically, being similar to the layered MoS_2, (002) preferred orientation layered $PbPdO_2$ has a small band gap [14], and the piezoresistive effect is expected.

In this work, based on the first-principle calculation method, a plane strain model was set up to obtain a deformed lattice with in-plane arbitrary uniaxial strain. In-plane anisotropy strain dependence of band-gap and carrier concentration were systematically investigated in the $PbPdO_2$ and $PbPd_{0.75}Co_{0.25}O_2$ slabs with preferred (002) orientation. These results can be well explained according to the p-d exchange interaction. Moreover, it is strongly suggested that the element-doping $PbPdO_2$ should become an important piezoresistance candidate material.

2. Methods

Based on Vienna ab initio simulation package (VASP), the self-consistent total energy was calculated and the geometry was optimized using the perdew-burke-ernzerhof (PBE) exchange-correlation functionals and the projector-augmented wave potentials [19,20]. The strain effect on the electronic properties of $PbPdO_2$ and $PbPd_{0.75}Co_{0.25}O_2$ slabs were simulated via standard DFT (Density functional theory) with generalized gradient approximation (GGA) method [21].

The cut-off energy was set to be 500 eV. The initial structure of $PbPdO_2$ and $PbPd_{0.75}Co_{0.25}O_2$ slabs were obtained from bulk $PbPdO_2$ and $PbPd_{0.75}Co_{0.25}O_2$, respectively [10,20]. Then, to make the in-plane force reach up to the minimum, both initial structures were totally relaxed through the energy minimization method. Starting with the relaxed initial structures of $PbPdO_2$ and $PbPd_{0.75}Co_{0.25}O_2$ slabs, the effects on the atoms and band structures were studied systematically under the strain with

the range of ±2%, which applied in the in-plane anisotropy uniaxial strain direction. The positive (negative) values of strain corresponded to the stretch and compression, respectively. The positions of all the atoms in the cell were relaxed by the optimizations of the strained structures with the Gaussians smearing method. After relaxation, each atom's convergence tolerance of force was smaller than 0.01 eV/Å. Meanwhile, 21 × 11 × 1 and 19 × 13 × 1 Monkhorst-Pack's meshes were used in the calculation of density of states (DOS) for $PbPdO_2$ and $PbPd_{0.75}Co_{0.25}O_2$ slabs, respectively.

3. Results and Discussion

Figure 1 shows the relaxed crystal structures of $PbPdO_2$ and $PbPd_{0.75}Co_{0.25}O_2$ ultrathin slabs with (002) preferred orientation. As shown in Figure 1, the unstrained $PbPdO_2$ and ultrathin slab revealed an in-plane symmetric configuration, maintaining the important properties of $PbPdO_2$. After Co-doping, the symmetric configuration of $PbPd_{0.75}Co_{0.25}O_2$ was broken. In comparison to the pristine $PbPdO_2$, the broken-symmetry in $PbPd_{0.75}Co_{0.25}O_2$ was expected to bring different physical properties. It should be noted that the anisotropy of $PbPd_{0.75}Co_{0.25}O_2$ was greatly affected by the state of the Co-substitution. Moreover, its configurations were fairly complicated. Here, the configuration with the least number of atoms and only one Co doping atom was considered, as seen in Figure 1b. Specifically, this Co atom forms square planar bonding with the nearest-neighbor four O atoms, which plays an important role on the electrical properties of $PbPd_{0.75}Co_{0.25}O_2$.

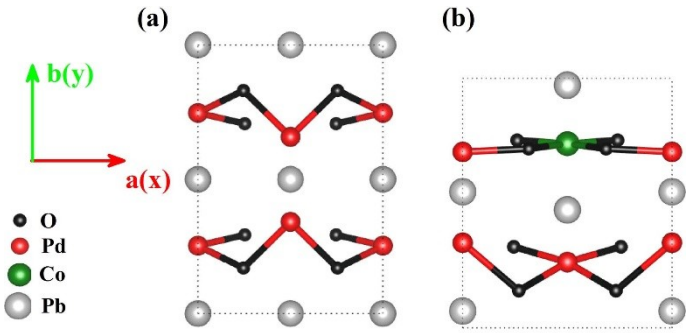

Figure 1. Top view of atomic structures in ab plane, (**a**) $PbPdO_2$, and (**b**) $PbPd_{0.75}Co_{0.25}O_2$ with (002) orientation.

Figure 2a–d shows the calculated electronic structures and the partial densities of states of Pb, Pd, O, and Co in $PbPdO_2$ and $PbPd_{0.75}Co_{0.25}O_2$ slabs, respectively. It was found that $PbPdO_2$ exhibits intrinsic characteristics of narrow band gap (0.051 eV), which was much smaller than that (0.4 eV) of the $PbPd_{0.75}Co_{0.25}O_2$ slab. In our previous experimental work, $PbPdO_2$ with (002) preferred orientation was prepared, and its band gap was found to be close to zero [22]. It is suggested that the localized Co would be responsible for the large band gap of 0.35 eV for the $PbPd_{0.75}Co_{0.25}O_2$ bulk material. Interestingly, our calculated results were consistent with the reported results [23]. The band gap of $PbPdO_2$ slab was slightly larger than that reported in our previous calculated work because of the different full in-plane structure relaxation [14]. From the density of electronic states in Figure 2b,d, it is found that DOSs of the pristine and Co-doped $PbPdO_2$ slabs at minimum of the conduction band and maximum of the valence band were mainly composed of 4d(Pd) and 2p(O) states. These results were similar to those found by many research groups [6,10]. In contrast, the $PbPd_{0.75}Co_{0.25}O_2$ slab had more distinct contribution of hybridization of 2p(O)–4d(Pd) states, where a Co 3d state added modified energy to the DOS at the Fermi energy level.

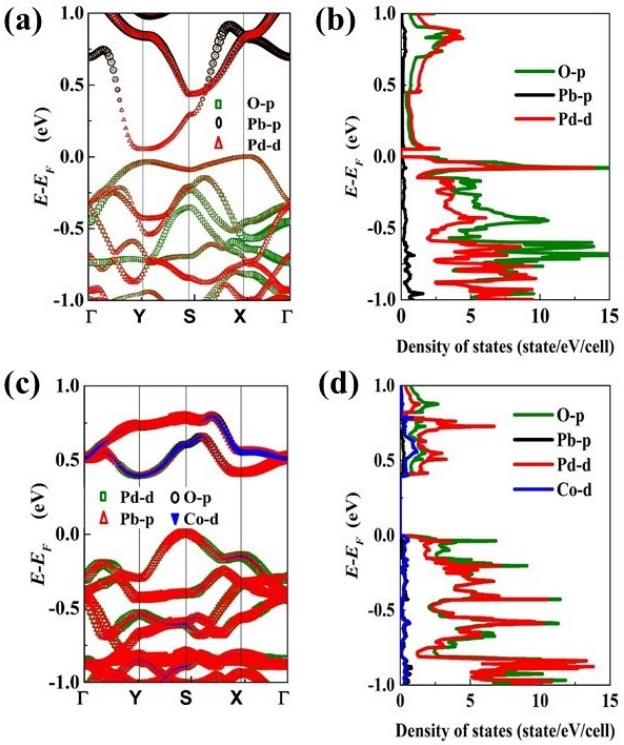

Figure 2. (**a**) electronic structures, and (**b**) orbital-resolved partial density of states (DOS) of (002) orientation $PbPdO_2$ slab; (**c**) electronic structures, and (**d**) orbital-resolved partial DOS of (211) orientation $PbPd_{0.75}Co_{0.25}O_2$ slab. The abscissa in (**a**,**c**) is the path of high symmetry points in Brillouin zone.

To gain insight into the potential mechanism of strain-induced electronic properties in $PbPdO_2$-base composites, a plane-stress-strain model was set up. Figure 3a,b present the undeformed lattice and a deformed lattice with in-plane arbitrary uniaxial tensile strain (directional cosines $(\cos\alpha, \cos\beta)$), respectively. The strain-related components could be obtained based on the coordinate transformation method. Assuming uniaxial strain ε is along the x′ direction in an unprimed coordinate system x-y, the strain tensor elements in the primed coordinate system are given as follows,

$$\begin{bmatrix} \varepsilon_x \\ \varepsilon_y \\ \gamma_{xy} \end{bmatrix} = \begin{bmatrix} l_1^2 & l_2^2 & l_1 l_2 \\ m_1^2 & m_2^2 & m_1 m_2 \\ 2l_1 m_1 & 2l_2 m_2 & l_1 m_2 + l_2 m_1 \end{bmatrix} \begin{bmatrix} \varepsilon_{x'} \\ \varepsilon_{y'} \\ \gamma_{x'y'} \end{bmatrix} \tag{2}$$

where $\varepsilon_{x'}(\varepsilon_{y'})$ and $\gamma_{x'y'}$ are normal (tensile or compressive) and shear strains, respectively [24]. The directional cosines are

$$l_1 = \cos\alpha,\ l_2 = \cos\alpha' \tag{3}$$

$$m_1 = \cos\beta,\ m_2 = \cos\beta' \tag{4}$$

where α, β, α', β' are arbitrary directions in the x-y and x′-y′ coordinate system, as seen in Figure 3.

A deformation of the unit cell is created by changing the Bravais lattice vectors R of the undeformed unit cell to R' using a strain matrix as follows:

$$R'(\alpha, \beta) = R \begin{bmatrix} 1+\varepsilon_x & \gamma_{xy} & 0 \\ \gamma_{xy} & 1+\varepsilon_y & 0 \\ 0 & 0 & 1 \end{bmatrix} \tag{5}$$

where R is the Bravais lattice vectors with strain, and R' is the Bravais lattice vectors without strain, $\varepsilon_x(\varepsilon_y)$ and $\gamma_{xy}(\gamma_{yx})$ are the normal (tensile or compressive) and shear strain-related components, respectively.

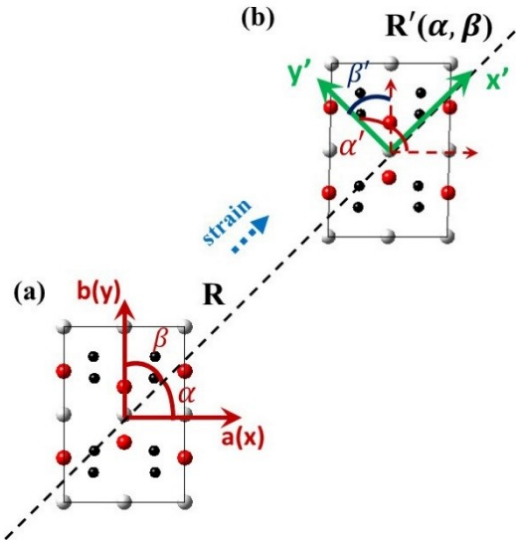

Figure 3. Diagram for (**a**) an undeformed lattice, (**b**) a deformed lattice with in-plane arbitrary uniaxial tensile strain (directional cosines $(\cos\alpha, \cos\beta)$).

Figure 4a,b shows the orientation distribution curves of band gap E_g with $\varepsilon = -0.02$, 0.00, 0.02 for the $PbPdO_2$ and $PbPd_{0.75}Co_{0.25}O_2$ slabs, respectively. It is clear that both slabs show a distinct anisotropy of gap with different strain. In Figure 4a, the $PbPdO_2$ slab shows the symmetrical and peanut-like $E_g - \alpha$ curves, and having the largest and smallest band-gap values along the x axis ($\alpha = 0°$) or y axis ($\alpha = 90°$), respectively. In contrast, as shown in Figure 4b, the $PbPd_{0.75}Co_{0.25}O_2$ slab has a maximum gap for the strain $\varepsilon = -0.02$ at about $\alpha = 75°$ and a minimum gap for the strain $\varepsilon = 0.02$ at about $\alpha = 0°$.

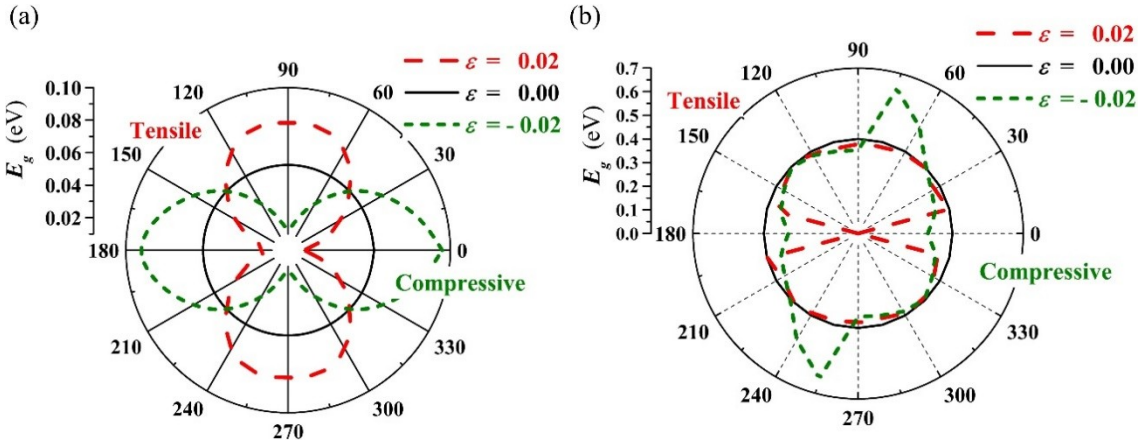

Figure 4. The orientation distribution curves of band gap E_g for (**a**) $PbPdO_2$, and (**b**) $PbPd_{0.75}Co_{0.25}O_2$ with $\varepsilon = -0.02$, 0.00, 0.02.

Figure 5a,b shows the band gap as a function of the strain for $PbPdO_2$ and $PbPd_{0.75}Co_{0.25}O_2$ along x axis ($\alpha = 0°$) and y axis ($\alpha = 90°$), respectively. As shown in Figure 5a, it is found that the band-gap value increases with increasing strain along the y-axis, whilst the band-gap value decreases with increasing strain along the x-axis. It is interesting that the band gap of the $PbPdO_2$ slab would widen when a compressive stress is applied closely to the x-axis or a tensile stress is applied closely to

the y-axis, as seen in Figure 4a. These calculated results can be explained according to the interaction of Pd–O bonding. It is expected that a compressive stress along the x-axis or tensile stress along the y-axis pulls O atoms apart from Pd atoms, which weakens the interaction of Pd and O. On the other hand, a tensile stress along the x-axis or compressive stress along the y-axis would push O atoms closely to Pd atoms and strengthen the interaction of Pd and O. As a result, the band gap is decreased. A similar result has also been reported in MoS_2 and black phosphorus [25,26].

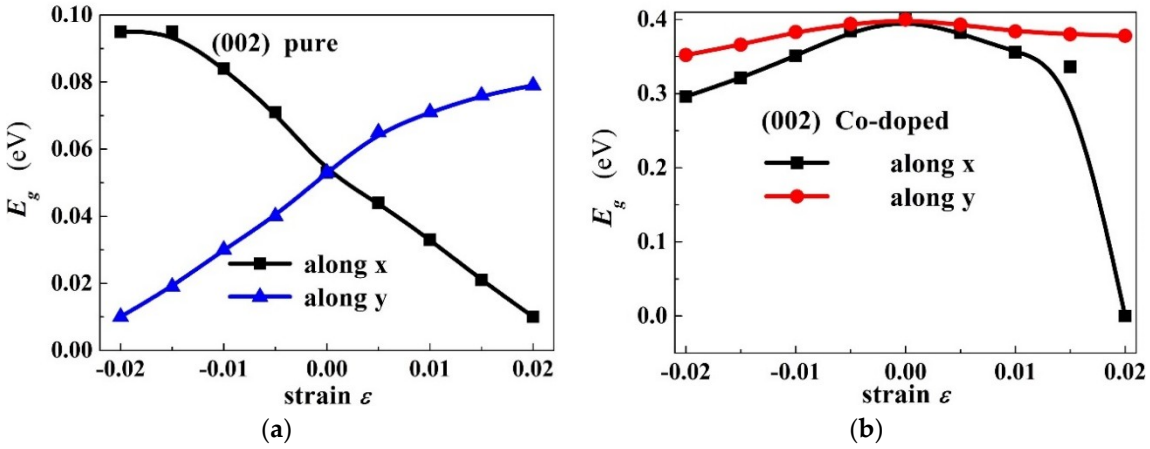

Figure 5. Band gap E_g as a function of strain for (**a**) $PbPdO_2$, and (**b**) $PbPd_{0.75}Co_{0.25}O_2$ along x-axis (called x) and b-axis (called y).

Figure 6 shows the plane averaged electron density difference $\Delta\rho$ of $PbPd_{0.75}Co_{0.25}O_2$ projected along the x axis and under $\varepsilon = -0.02$, with $\alpha = 15°$, 45°, 75°, and 90°, respectively. In comparison, it is found that p-d charge transfer $\Delta\rho$ between Co and O exhibits an evident change for $\alpha = 75°$. Therefore, the band gap of $PbPd_{0.75}Co_{0.25}O_2$ is expected to be changed significantly as the compressive stress direction is along a particular direction with $\alpha = 75°$. Figure 7 shows the plane averaged electron density difference $\Delta\rho$ of $PbPd_{0.75}Co_{0.25}O_2$ projected along the x axis under $\varepsilon_x = -0.02$, -0.01, 0.00, 0.01, 0.02, respectively. Based on spin-splitting theory, the minimum gap of the $PbPd_{0.75}Co_{0.25}O_2$ slab with the strain $\varepsilon_x = 0.02$ is strongly related to the variation of $\Delta\rho$. From Figure 7, it is concluded that Co atom should act as the source of the localized magnetic moment, and the coupling between the p-state from O and d-state from Co could induce a strong exchange interaction (named as p-d exchange interaction) in $PbPd_{0.75}Co_{0.25}O_2$. Moreover, the p-d exchange interaction was found to be nearly inversely proportional to the unit cell volume [27]. Therefore, p-d exchange interaction mediated by strain should be responsible for variation of the plane averaged electron density difference, leading to a clear change of the band gap.

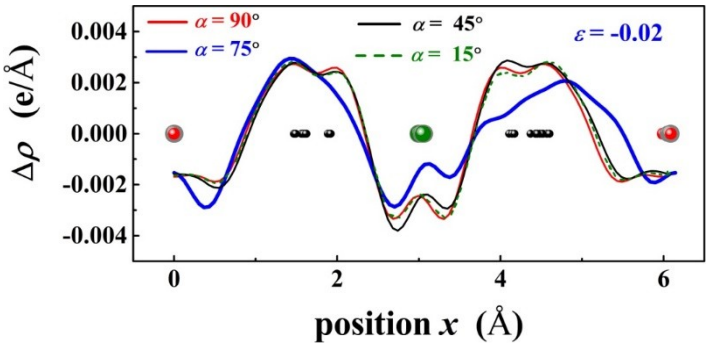

Figure 6. The plane averaged electron density difference $\Delta\rho$ of $PbPd_{0.75}Co_{0.25}O_2$ projected along the x axis and under $\varepsilon = -0.02$, with $\alpha = 15°$, 45°, 75°, and 90°, respectively.

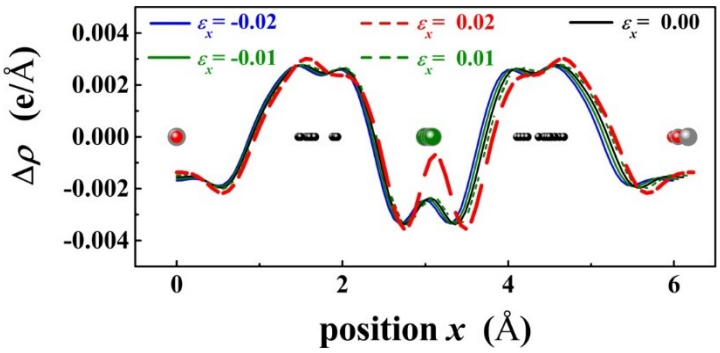

Figure 7. The plane averaged electron density difference $\Delta\rho$ of $PbPd_{0.75}Co_{0.25}O_2$ under $\varepsilon_x = -0.02$, -0.01, 0.00, 0.01, 0.02, where the projection of $\Delta\rho$ was along the x axis.

Figure 8 shows the spin polarized total density states of the $PbPd_{0.75}Co_{0.25}O_2$ slab with different strain along the x and y-axes external uniaxial strain directions. From the figure, it is found that the spin-up and spin-down DOSs are asymmetric, which means the existence of magnetic moment. The magnetic properties in element doped $PbPdO_2$ will be studied in subsequent research work. Interestingly, as shown in Figure 8e, the tensile strain with ε_x = 0.02 leads to the zero-band gap structure. The strain gives rise to the evident left shift of the bottom of the conduction band in spin-down DOSs, which effectively modulates the band gap. When the strain is large enough, the top of the valence band and the bottom of the conduction band in spin-up and spin-down DOSs all shift with changing strain, which leads to clear modulation of the band gap. This interesting phenomenon is similar to the fact that the slight tensile strain results in the zero-band gap structure [4].

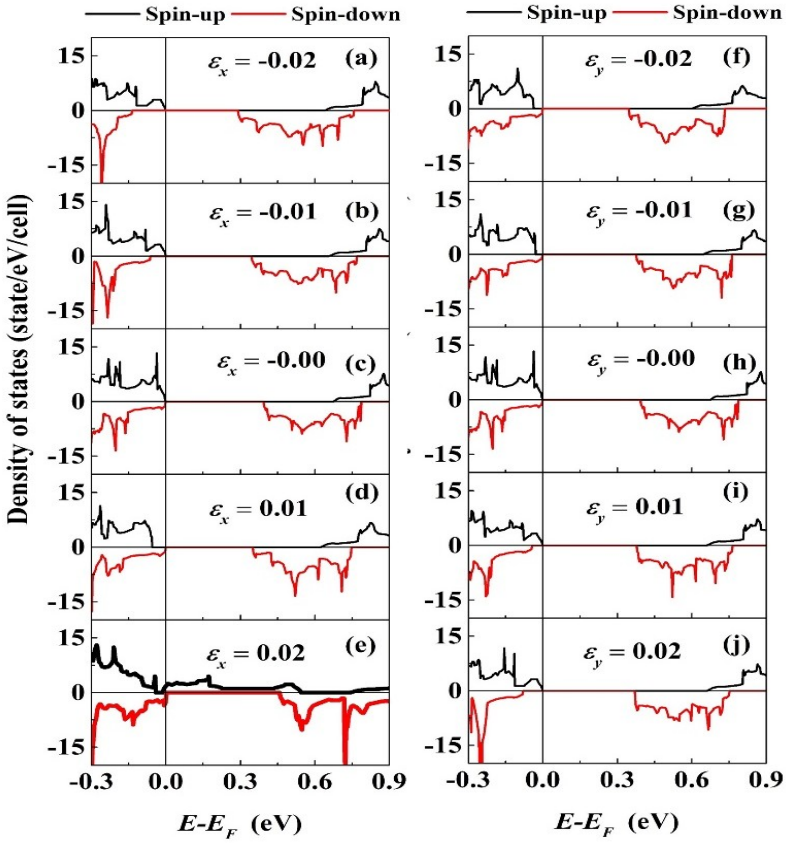

Figure 8. The spin polarized total density states of the $PbPd_{0.75}Co_{0.25}O_2$ slab with different strain $\varepsilon_x(\varepsilon_y)$: (**a**–**e**) along the x-axis, and (**f**–**j**) along the y-axis external uniaxial strain directions.

Unique electrical properties are highly desirable for practical application, and charge carrier concentration is a key parameter for the intrinsic semiconductor. For the intrinsic semiconductor, the charge charier concentration can be estimated as follows [28],

$$n \propto T^{3/2} \exp\left[-\frac{E_g}{2K_B T}\right] \tag{6}$$

$$n_\varepsilon / n_0 \propto \exp\left[-\frac{\Delta E_g}{2K_B T}\right] = \exp\left[-\frac{E_g - E_{g0}}{2K_B T}\right] \tag{7}$$

where K_B, E_g are the Boltzmann constant and band gap, respectively. In this paper, all the temperatures in carrier concentration were calculated at T = 100 K. As $\varepsilon = 0$, let $n = n_0$; $\varepsilon \neq 0$, let $n = n_\varepsilon$.

Combined with the results presented in Figure 4a,b, the external strain dependence of charge carrier concentration ratio (n_ε / n_0) for $PbPdO_2$ and $PbPd_{0.75}Co_{0.25}O_2$ slabs were evaluated, respectively. Figure 9a,b shows the orientation distribution curves of the intrinsic charge carrier concentration ratio n/n_0 for $PbPdO_2$ and $PbPd_{0.75}Co_{0.25}O_2$ slabs with $\varepsilon = -0.02, -0.01, 0.00, 0.01, 0.02$, respectively. Similar to the dependence of band gap E_g on strain orientation, $PbPd_{0.75}Co_{0.25}O_2$ exhibits more distinct anisotropy in carrier concentration with strain direction, especially along the x-axis. As shown in Figure 9a, the pristine $PbPdO_2$ slab demonstrates the symmetrical and olive-like $(n_\varepsilon / n_0)_{-\alpha}$ curves, and having its largest and smallest band-gap values along the x-axis or y-axis, respectively. For the $PbPd_{0.75}Co_{0.25}O_2$ slab, the carrier concentration is sensitive to the application direction of strain. When the compressive stress applies along a direction of 75° ($\alpha \approx 75°$) and x-axis, the remarkable variety in carrier concentration appears, as shown in Figure 9b. Figure 10c,d shows the intrinsic charge carrier concentration ratio $(n_\varepsilon - n_0)/n_0$ as a function of strain for $PbPdO_2$ and $PbPd_{0.75}Co_{0.25}O_2$ slabs along the x and y-axes, respectively. For the $PbPdO_2$ slab, the carrier concentration increases monotonically with increasing compressive stress, but decreasing with increasing tensile stress along the x-axis. On the contrary, the carrier concentration decreases with increasing compressive stress, while increasing with increasing tensile stress along the y-axis. In contrast, the carrier concentration of $PbPd_{0.75}Co_{0.25}O_2$ slab increases with increasing compressive and tensile stresses along both the x and y-axes. As the compressive stress increases beyond 0.015 along the x-axis, carrier concentration of the $PbPd_{0.75}Co_{0.25}O_2$ slab increases rapidly. It was found that the carrier concentration of $PbPd_{0.75}Co_{0.25}O_2$ could sharply increase up to 5–6 orders of magnitude with the help of external strain with ε = 0.02. The calculated results suggest strongly that the element-doping $PbPdO_2$ should become an important piezoresistance candidate material.

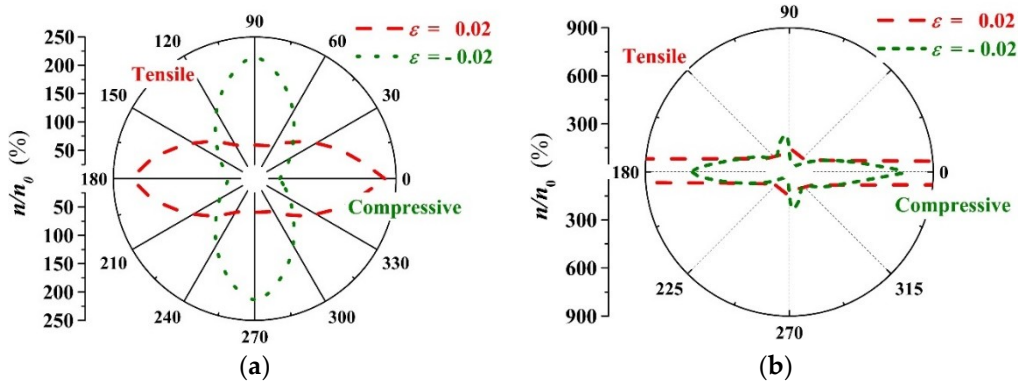

Figure 9. The orientation distribution curves of intrinsic charge carrier concentration ratio n/n_0 for (**a**) $PbPdO_2$, and (**b**) $PbPd_{0.75}Co_{0.25}O_2$ with $\varepsilon = -0.02$ and 0.02.

Figure 11 presents the strain dependence of gauge factor for the $PbPdO_2$ and $PbPd_{0.75}Co_{0.25}O_2$ slab along the x and y axes. Table 1 gives some typical gauge factor values. When the tensile strain is 0.02, the piezoresistive gauge factors for the $PbPdO_2$ and $PbPd_{0.75}Co_{0.25}O_2$ slab along the x-axis

are calculated to be respectively 62.8 and −43.3, which is comparable to trilayer MoS_2 and much higher than suspended-graphene-based strain sensor [29]. As Pd–O (Co–O) polar covalent bond is different from C–C bond, $PbPdO_2$-based semiconductors can exhibit a higher piezoresistive gauge factor than graphene-based strain sensors. The predicted large gauge factors in our work implies that the element-doping $PbPdO_2$ may have promising opportunities to be used as strain sensors.

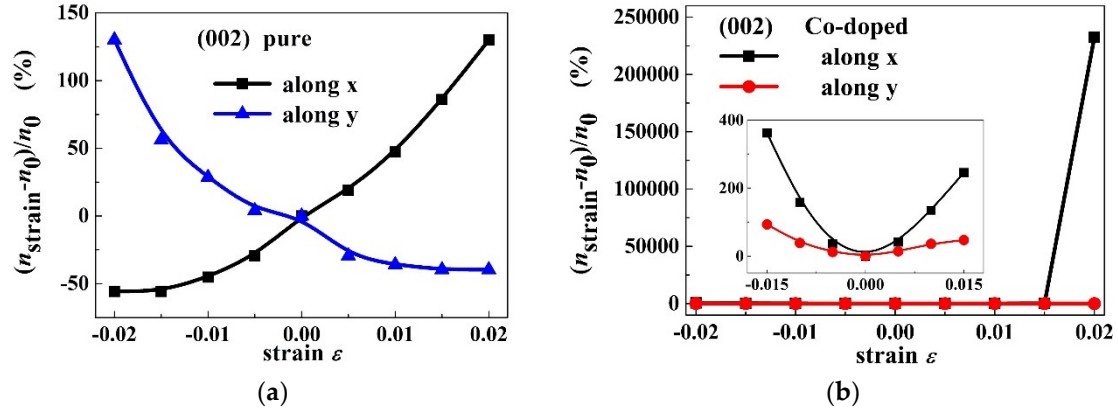

Figure 10. The intrinsic charge carrier concentration ratio $(n_\varepsilon - n_0)/n_0$ as a function of strain for (**a**) $PbPdO_2$, and (**b**) $PbPd_{0.75}Co_{0.25}O_2$ along the a-axis (called x) and b-axis (called y) with $\varepsilon = -0.02$ and 0.02. The inset shows a magnification curve with strain ranges from −0.015 to 0.015.

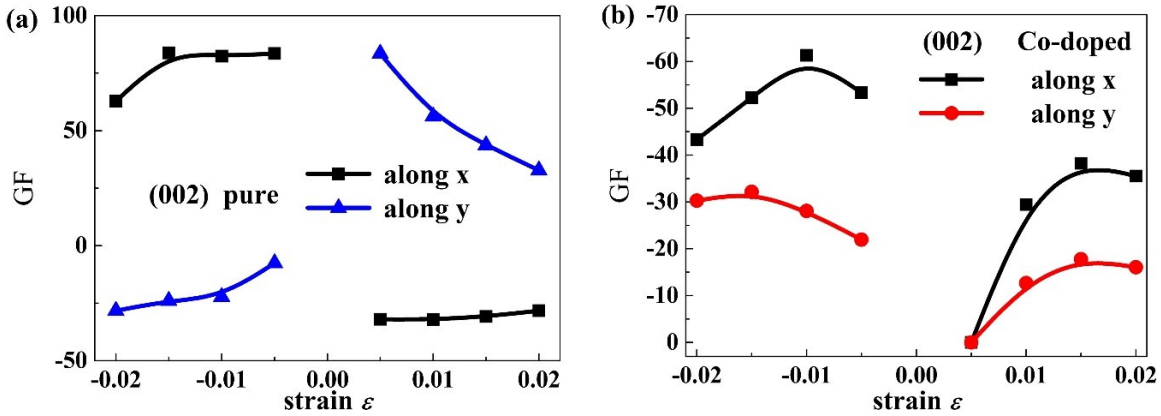

Figure 11. The piezoresistive gauge factor as a function of strain for (**a**) $PbPdO_2$, and (**b**) $PbPd_{0.75}Co_{0.25}O_2$ along the x and y axes.

Table 1. Some typical gauge factors of $PbPdO_2$ and $PbPd_{0.75}Co_{0.25}O_2$ along the x and y axes.

Typical Gauge Factors	$PbPdO_2$ Slab				$PbPd_{0.75}Co_{0.25}O_2$ Slab			
	Direction							
	x		y		x		y	
ε	−0.02	0.02	−0.02	0.02	−0.02	0.02	−0.02	0.02
GF	62.8	−28.3	−28.3	32.8	−43.3	−35.5	−30.3	−16.1

4. Conclusions

Based on first-principles calculations, the electronic structures and electrical properties of $PbPdO_2$ and $PbPd_{0.75}Co_{0.25}O_2$ ultrathin slabs were systematically investigated. The calculated results indicated that the strain induces changes of band structure and carrier concentration in both slabs. Specifically, the carrier concentration of the $PbPd_{0.75}Co_{0.25}O_2$ slab could be modulated with 5–6 orders externally induced strain, which renders the Co-doped pristine $PbPdO_2$ phase a potentially promising

piezoresistive material. Moreover, the above evident external strain modulation of the band gap and carrier concentration can be well explained by spin-splitting theory.

Author Contributions: Conceptualization, Y.Y., J.Z. and Z.H.; Methodology, Y.Y. and J.Z.; Formal Analysis, Y.Y., J.Z., K.Z. and Z.H.; Investigation, Y.Y., J.Z., G.X. and Z.H.; Writing—Original Draft Preparation, Y.Y., J.Z. and Z.H.; Writing—Review & Editing, Z.H.

Acknowledgments: This work was supported by the National Science Foundation of China (Nos. 61574037, 61804030, 11874113) and the Natural Science Foundations of Fujian Province of China (Nos. 2017J06001, 2016J05151, 2016J01011). G.X. would like to thank the support from Fujian Provincial College Funds for Distinguished Young Scientists of year 2015.

Conflicts of Interest: The authors declare no conflict of interest.

References

1. Armand, M.; Tarascon, J.-M. Building better batteries. *Nature* **2008**, *451*, 652–657. [CrossRef] [PubMed]
2. Ouardi, S.; Fecher, G.H.; Felser, C. Realization of spin gapless semiconductors: The Heusler compound Mn_2CoAl. *Phys. Rev. Lett.* **2013**, *110*, 100401. [CrossRef] [PubMed]
3. Bainsla, L.; Mallick, A.I.; Raja, M.M.; Coelho, A.A.; Nigam, A.K. Origin of spin gapless semiconductor behavior in CoFeCrGa: Theory and experiment. *Phys. Rev. B* **2015**, *92*, 045201. [CrossRef]
4. Wang, X.L. Proposal for a new class of materials: Spin gapless semiconductors. *Phys. Rev. Lett.* **2008**, *100*, 156404. [CrossRef] [PubMed]
5. Wang, X.L.; Peleckis, G.; Zhang, C.; Kimura, H.; Dou, S. Colossal electroresistance and giant magnetoresistance in doped $PbPdO_2$ thin films. *Adv. Mater.* **2009**, *21*, 2196–2199. [CrossRef]
6. Wang, X.L. Dirac spin-gapless semiconductors: promising platforms for massless and dissipationless spintronics and new (quantum) anomalous spin Hall effects. *Nat. Sci. Rev.* **2017**, *4*, 252–257. [CrossRef]
7. Lee, K.S.; Choo, S.M.; Jung, M.-H. Magnetic versus nonmagnetic ion substitution effects in gapless semiconductor $PbPdO_2$. *Appl. Phys. Lett.* **2015**, *106*, 072406. [CrossRef]
8. Tang, F.L.; Liu, J.; Mei, C.; Huang, S.Y.; Song, T.T.; Su, H.L.; Lee, M.K.; Wu, Y.C.; Huang, J.C.A. Microstructure and magnetism of Co-doped $PbPdO_2$ films with different grain sizes. *RSC Adv.* **2016**, *6*, 37522–37529. [CrossRef]
9. Choo, S.M.; Lee, K.J.; Park, S.M.; Yoon, J.B.; Park, G.S.; You, C.-Y.; Jung, M.H. Crossover between weak anti-localization and weak localization by Co doping and annealing in gapless $PbPdO_2$ and spin gapless Co-doped $PbPdO_2$. *Appl. Phys. Lett.* **2014**, *106*, 172404. [CrossRef]
10. Chen, S.W.; Huang, S.C.; Guo, G.Y.; Lee, J.M.; Chiang, S.; Chen, W.C.; Liang, Y.C.; Lu, K.T.; Chen, J.M. Gapless band structure of $PbPdO_2$: A combined first principles calculation and experimental study. *Appl. Phys. Lett.* **2011**, *99*, 012103. [CrossRef]
11. Srivastava, P.; Nagare, B.J.; Kanhere, D.G.; Sen, P. Electronic structure of the spin gapless material Co-doped $PbPdO_2$. *J. Appl. Phys.* **2013**, *114*, 103709. [CrossRef]
12. Liu, J.; Mei, C.; Chuang, P.Y.; Song, T.T.; Tang, F.L.; Su, H.L.; Huang, J.C.A.; Wu, Y.C. Effect of Fe doping on the magnetic properties of $PbPdO_2$ nanograin film fabricated by sol-gel method. *Ceram. Int.* **2016**, *42*, 15762–15766. [CrossRef]
13. Kim, D.H.; Hwang, J.; Lee, E.; Lee, K.J.; Choo, S.M.; Jung, M.H.; Baik, J.; Shin, H.J.; Kim, B.K.; Min, B.I.; et al. Valence states and electronic structures of Co and Mn substituted spin gapless semiconductor $PbPdO_2$. *Appl. Phys. Lett.* **2014**, *104*, 022411. [CrossRef]
14. Yang, Y.M.; Zhong, K.H.; Xu, G.G.; Zhang, J.-M.; Huang, Z.G. Electronic structure and its external electric field modulation of $PbPdO_2$ ultrathin slabs with (002) and (211) preferred orientations. *Sci. Rep.* **2017**, *7*, 6898. [CrossRef] [PubMed]
15. Peng, X.; Wei, Q.; Copple, A. Strain-engineered direct-indirect band gap transition and its mechanism in two-dimensional phosphorene. *Phys. Rev. B* **2014**, *90*, 085402. [CrossRef]
16. Kanda, Y. Piezoresistance effect of silicon. *Sens. Actuators A Phys.* **1991**, *28*, 83–91. [CrossRef]
17. Wu, W.; Wang, L.; Li, Y.; Zhang, F.; Lin, L.; Niu, S.; Chenet, D.; Zhang, X.; Hao, Y.; Heinz, T.F.; et al. Piezoelectricity of single-atomic-layer MoS_2 for energy conversion and piezotronics. *Nature* **2014**, *514*, 470–474. [CrossRef] [PubMed]

18. Manzeli, S.; Allain, A.; Ghadimi, A.; Kis, A. Piezoresistivity and strain-induced band gap tuning in atomically thin MoS_2. *Nano Lett.* **2015**, *15*, 5330–5335. [CrossRef] [PubMed]
19. Kresse, G.; Furthmüller, J. Efficiency of ab-initio total energy calculations for metals and semiconductors using a plane-wave basis set. *Comput. Mater. Sci.* **1996**, *6*, 15–50. [CrossRef]
20. Kresse, G.; Furthmüller, J. Self-interaction correction to density functional approximation for many electron systems. *Phys. Rev. B* **1996**, *54*, 11169–11186. [CrossRef]
21. Perdew, J.P.; Burke, K.; Ernzerhof, M. Generalized gradient approximation made simple. *Phys. Rev. Lett.* **1996**, *77*, 3865–3868. [CrossRef] [PubMed]
22. Chen, X.; Chen, Y.; Yang, Y.M.; Jia, H.; Zhang, J.M.; Chen, S.Y.; Huang, Z.G. The structure and electrical properties of $PbPdO_2$ thin films with preferred orientation prepared by PLD. *Ceram. Int.* **2017**, *43*, 10428–10433. [CrossRef]
23. Chen, S.W.; Huang, S.C.; Guo, G.Y.; Lee, J.M.; Chiang, S.; Chen, W.C.; Liang, Y.C.; Lu, K.T.; Chen, J.M. A combined first principle calculations and experimental study on the spin-polarized band structure of Co-doped $PbPdO_2$. *Appl. Phys. Lett.* **2012**, *101*, 222104. [CrossRef]
24. Chen, H.; Huang, P.; Guo, D.; Xie, G.X. Anisotropic mechanical properties of black phosphorus nanoribbons. *J. Phys. Chem. C* **2016**, *120*, 29491–29497. [CrossRef]
25. Li, C.; Fan, B.; Li, W.-Y.; Wen, L.-W.; Liu, Y.T.; Sheng, W.K.; Yin, Y. Band gap engineering of monolayer MoS_2 under strain: A DFT study. *J. Korean Phys. Soc.* **2015**, *66*, 1789–1793. [CrossRef]
26. Rafael, R.; Andrés, C.-G.; Emmanuele, C.; Francisco, G. Strain engineering in semiconducting two-dimensional crystals. *J. Phys. Condens. Matter* **2015**, *27*, 313201.
27. Dietl, T.; Ohno, H.; Matsukura, F. Hole-mediated ferromagnetism in tetrahedrally coordinated semiconductors. *Phys. Rev. B* **2001**, *63*, 195205. [CrossRef]
28. Grosso, G.; Parravicini, G.P. *Solid State Physics*, 2nd ed.; Academic Press: Amsterdam, The Netherlands, 2014; pp. 577–582. ISBN 978-0-120385030-0.
29. Smith, A.D.; Niklaus, F.; Paussa, A.; Vaziri, S.; Fischer, A.C.; Sterner, M.; Forsberg, F.; Delin, A.; Esseni, D.; Palestri, P.; et al. Electromechanical piezoresistive sensing in suspended graphene membranes. *Nano Lett.* **2013**, *13*, 3237. [CrossRef] [PubMed]